



HAL
open science

Continuous electroconversion of CO₂ into formate using 2 nm tin oxide nanoparticles

Ivan Merino-Garcia, Lionel Tinat, Jonathan Albo, Manuel Alvarez-Guerra,
Angel Irabien, Olivier Durupthy, Vincent Vivier, Carlos M Sánchez-Sánchez

► **To cite this version:**

Ivan Merino-Garcia, Lionel Tinat, Jonathan Albo, Manuel Alvarez-Guerra, Angel Irabien, et al.. Continuous electroconversion of CO₂ into formate using 2 nm tin oxide nanoparticles. Applied Catalysis B: Environmental, 2021, 297, pp.120447. 10.1016/j.apcatb.2021.120447 . hal-03267685

HAL Id: hal-03267685

<https://hal.sorbonne-universite.fr/hal-03267685v1>

Submitted on 22 Jun 2021

HAL is a multi-disciplinary open access archive for the deposit and dissemination of scientific research documents, whether they are published or not. The documents may come from teaching and research institutions in France or abroad, or from public or private research centers.

L'archive ouverte pluridisciplinaire **HAL**, est destinée au dépôt et à la diffusion de documents scientifiques de niveau recherche, publiés ou non, émanant des établissements d'enseignement et de recherche français ou étrangers, des laboratoires publics ou privés.

Continuous electroconversion of CO₂ into formate using 2 nm tin oxide nanoparticles

Ivan Merino-Garcia^{a,b,c}, Lionel Tinat^d, Jonathan Albo^b, Manuel Alvarez-Guerra^b, Angel Irabien^b, Olivier Durupthy^d, Vincent Vivier^c, Carlos M. Sánchez-Sánchez^{c,*}

^a Universidade Nova de Lisboa, FCT, Chemistry Department, Associated Laboratory for Green Chemistry-Clean Technologies and Processes (LAQV), Caparica 2829-516, Portugal

^b University of Cantabria, Department of Chemical and Biomolecular Engineering, Avenida de los Castros s/n, 39005 Santander, Cantabria, Spain

^c Sorbonne Université, CNRS, Laboratoire Interfaces et Systèmes Electrochimiques, LISE, 4 place Jussieu, F-75005 Paris, France

^d Sorbonne Université, CNRS, Collège de France, Laboratoire de Chimie de la Matière Condensée de Paris, 4 place Jussieu, F-75005 Paris, France

* Corresponding author; e-mail: carlos.sanchez@upmc.fr

Abstract

Tin oxide nanoparticles (SnO₂ NPs) as electrocatalyst for the production of formate from CO₂ reduction reaction (CO₂RR). We synthesize, characterize and evaluate high surface area SnO₂ NPs (2.4 nm and 299 m² g⁻¹ in diameter size and surface area, respectively), for the continuous production of formate at high current density within a flow electrolyzer.

SnO₂ NPs under Ar and CO₂ reduction conditions were studied by cyclic voltammetry. SnO₂-based gas diffusion electrodes (SnO₂-GDEs) were manufactured to perform continuous CO₂RR. A maximum formate concentration value of 27 g L⁻¹ was achieved with a Faradaic efficiency (FE) of 44.9% at 300 mA cm⁻², which was significantly stable and reproducible when operated up to 10 h. Nevertheless, ohmic drop contribution due to the semiconducting properties of SnO₂ was not negligible. The low total FE (< 60%) of products pointed out a leakage of formate by crossover migration through the membrane from the catholyte towards the anolyte.

Keywords: CO₂ electroreduction, formate, SnO₂ nanoparticles, Continuous reactor, Gas diffusion electrodes.

1. Introduction

The concentration of CO₂ in the atmosphere is reaching unprecedented values (413 ppm in December 2020) [1] due to the increasing depletion of fossil fuels as world energy demand continues to increase. Thus, the conversion of captured CO₂ into useful chemicals is considered one of the most efficient technologies to tackle the challenge [2–4]. Although several CO₂ activation and conversion techniques are nowadays available such as chemical, photochemical

1 and photoelectrochemical methods [5–7], the catalytic process for the transformation of CO₂
2 into value-added products throughout electrochemical reactions is appealing due to the
3 environmental and potential economic benefits. In particular, the possibility of closing the carbon
4 cycle, as well as its strategic advantage in storing electrical energy in the form of chemical
5 bonds, makes this technology one of the most sustainable methods currently available, in which
6 the electrons can be derived from renewable energy sources such as wind or solar power [8].
7 For this reason, different approaches from both homogeneous [9–11] and heterogeneous
8 catalysis [12,13] have been applied to the electrochemical CO₂ reduction reaction (CO₂RR).

9 Different commercially useful chemicals can be produced from the electrochemical conversion
10 of CO₂ at room temperature as a function of the number of proton-coupled electron transfers
11 required in each electrochemical reaction [14–17]. In addition to this, the selectivity of the
12 reaction strongly depends on the catalytic material, as well as process conditions, such as the
13 applied voltage, among others [18,19]. The main products obtained from CO₂ electroreduction
14 can be classified in the following four categories: *i*) carbon monoxide (CO) [20,21]; *ii*) formic
15 acid/formate (HCOOH/HCOO⁻) depending on the pH [22,23]; *iii*) alcohols such as methanol
16 (CH₃OH) [24] and ethanol (C₂H₅OH) [25]; and *iv*) hydrocarbons including methane (CH₄) [26]
17 and ethylene (C₂H₄) [27]. It is vital to stress the importance of controlling the hydrogen evolution
18 reaction (HER) [28], since the production of hydrogen from water electrolysis competes with
19 CO₂ electroconversion, reducing, therefore, the selectivity of the electrochemical process
20 towards the desired useful reduction product.

21 In this work, we study the continuous production of formate from CO₂ single-pass
22 electrochemical conversion, in which two electrons are exchanged, at high current density
23 within a flow electrolyzer, which allows direct feed of gaseous CO₂ to the electrochemical
24 interface by means of a gas diffusion cathode and avoids mass limitations associated with CO₂
25 solubility in solution. Formate is a widely used chemical commodity in different pharmaceutical
26 or leather industries, among others [22]. Moreover, formate can be supplied as fuel (starting
27 from 0.5 M in solution) for direct formic acid fuel cells (DFAFCs) to produce electricity [29] and is
28 considered one of the highest value-added CO₂ electroreduction products in terms of market
29 price since this chemical reaches a value of around \$1000 - \$1700 per ton of product [30]. The
30 main targets pointed out in the literature for the CO₂RR-into-formate process to become
31 industrially feasible are [31]: *i*) reaching a formate production higher than 45 g L⁻¹ (1 M); *ii*) using
32 current densities higher than 100 mA cm⁻²; *iii*) keeping Faradaic efficiency (FE) higher than 50%
33 and energy consumption lower than 500 kWh kmol⁻¹ product; and *iv*) using continuous-flow
34 operation mode at mild-ambient temperature and pressure conditions. Moreover, the long-term
35 stability and durability of the working electrodes have been recently reported to be crucial for
36 this technology to be implemented in the short term [32] and further comprehensive durability
37 tests are still needed in the literature.

38 Among the different available electrocatalysts mainly producing formate from CO₂RR, metallic
39 tin (Sn) appears to be one of the best alternatives in terms of cost and selectivity, highlighting

1 also its low toxicity, even though other metals such as lead (Pb) and bismuth (Bi) have also
2 been proposed as efficient electrocatalysts for formate production [23,33–37]. Nevertheless, not
3 only the synthesis of small size capping agent free Sn nanoparticles (NPs) is tricky, but also the
4 structural stability of Sn NPs during CO₂ electroreduction is under debate. Furthermore, the
5 behavior of Sn NPs under industrial (high) cathode area and current density conditions
6 represents a challenge that still needs to be solved [38]. As a consequence, either the use of
7 oxide films on Sn electrodes or purely tin oxide (SnO₂) NPs has been recently considered in
8 literature as suitable electrocatalytic material for the production of formate from CO₂RR [39–47],
9 since SnO₂ presents much higher structural stability under electrochemical conditions. In
10 particular, a lot of attention has been focused on identifying the role of the different species
11 present on the surface of the electrode (Sn/SnO/SnO₂) during CO₂RR. This surface
12 composition-reactivity relationship has been studied in detail by Raman and IR spectroscopy
13 [48–50] and scanning electrochemical microscopy (SECM) [51], which have demonstrated that
14 oxide films (SnO_x) on the surface of Sn electrodes play a key role by enhancing formate
15 production and selectivity during CO₂RR.

16 Therefore, the present study aims at evaluating the application of crystalline and high specific
17 surface area SnO₂ NPs (2.4 nm in average diameter size), synthesized by a template free and
18 facile hydrothermal microwave-assisted method, as an alternative electrocatalyst for the
19 continuous CO₂RR into formate at high current densities. As far as the authors know, this study
20 represents one of the first approaches on evaluating the activity and selectivity performance of
21 SnO₂ NPs smaller than 3 nm in a gas-phase flow electrolyzer using large size electrodes (10
22 cm² of geometrical area) operating at high current densities. This strategy has been recently
23 proposed with the purpose of increasing the formate production rates using 100 nm SnO₂
24 nanoparticles [52,53] and alternative larger size tin oxide-based electrocatalysts such as SnO
25 [54] or Sn₃O₄ [55]. Nevertheless, most of the work published so far has used SnO₂ catalyzed
26 gas diffusion electrodes (GDEs) in a two compartments H-type cell, where poor current
27 densities between 5 and 12.5 mA cm⁻² were reported [42,43,45,46,56]. Only highly porous SnO₂
28 nanosheets supported on carbon cloth reached 70 mA cm⁻² as current density in H-type cell
29 [57]. Therefore, we would like to evaluate large size SnO₂-GDEs capable of operating at
30 extreme current densities (*i.e.*, 500 mA cm⁻²) conditions in a gas-phase flow electrolyzer. Thus,
31 the following objectives are addressed herein: *i*) synthesis and comprehensive physicochemical
32 characterization of high surface area SnO₂ NPs; *ii*) electrochemical characterization of SnO₂
33 NPs deposited onto a glassy carbon electrode by cyclic voltammetry; *iii*) manufacturing of GDEs
34 as cathodes containing SnO₂ NPs as catalyst; and *iv*) analysis of the synthesized SnO₂-GDE
35 for the continuous CO₂RR into formate in aqueous solution, using a single-pass flow reactor
36 configuration [58–60] to evaluate their performance operating at high current densities.

37 **2. Experimental**

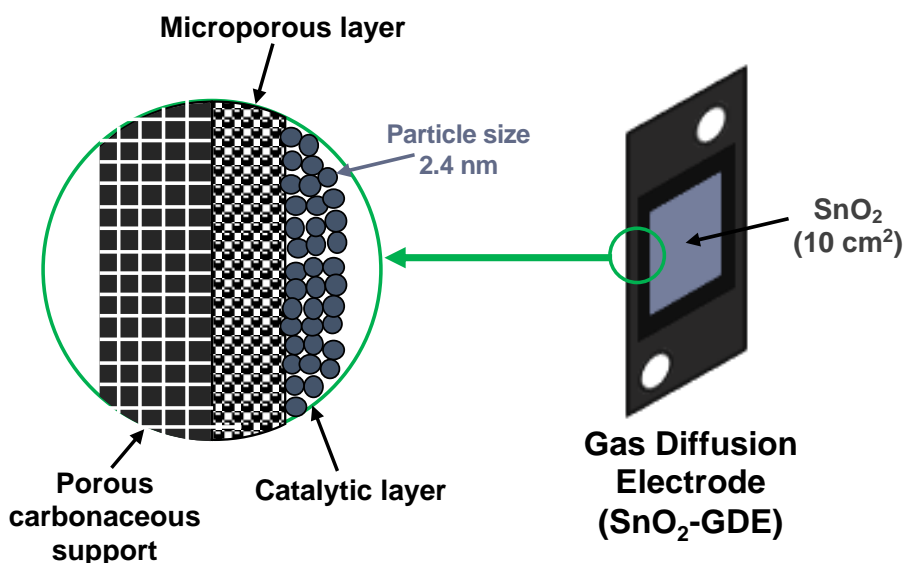
38 *2.1. Synthesis of SnO₂ nanoparticles*

1 The synthesis of the SnO₂ NPs has been carried out by a hydrothermal microwave-assisted
2 method [61,62]. In particular, a 0.1 mol L⁻¹ fresh aqueous solution of Sn (IV) was prepared by
3 adding 3.506 g of SnCl₄·5H₂O to 100 ml (pH = 2). Subsequently, 50 ml of that solution were
4 poured in a glass vial and transferred to a monomode microwave oven (Sairem Miniflox
5 200SS). The solution was then heated at 80 °C for 1 h under magnetic stirring (a maximum of
6 20 W was applied to maintain that temperature). The suspension was afterwards cooled to
7 room temperature in few minutes. The obtained white powder was washed by centrifugation
8 (three times with water and once with ethanol) for 20 min. Finally, a part of the powder was
9 dried during 15 h at room temperature under vacuum to carry out the physicochemical
10 characterization analyses. The remaining part of the powder was dispersed in isopropanol (1.33
11 g_{SnO₂} L⁻¹) to be used as the electrocatalyst in CO₂ electroreduction experiments.

12

13 *2.2. Gas diffusion electrodes manufacturing*

14 The preparation of SnO₂-GDEs was carried out according to the following procedure: initially, a
15 carbon-based ink is prepared by mixing carbon powder (Vulcan XC-72R, Cabot, carbon black),
16 and polytetrafluoroethylene (PTFE) (Sigma-Aldrich, 60 wt% dispersion in H₂O) in a mass ratio
17 40/60. The mixture was then diluted to 3% in isopropanol. The resulting dispersion was
18 airbrushed onto a carbonaceous gas diffusion layer (TGP-H-60 with 40% (w/w) PTFE, Toray
19 Inc.) supported on a Sn mesh current collector in order to obtain a partially hydrophobic carbon
20 microporous layer (MPL), which was finally sintered at 623 K for 30 min, following a procedure
21 previously described in recent contributions from some of the authors [63,64] (see Figure S3).
22 Then, a catalytic ink containing the synthesized SnO₂ NPs dispersed in isopropanol and a
23 Nafion solution (5 wt%, Alfa Aesar, copolymer polytetrafluoroethylene) with a
24 (SnO₂+Nafion)/isopropanol mass ratio of 1.6/98.4 was finally airbrushed onto the MPL surface.
25 The geometric surface area (A) of the catalytic layer was 10 cm² and the catalytic loading was
26 0.75 mg SnO₂ cm⁻², which were selected according to previous research studies using Sn-
27 GDEs [65]. The final catalyst loading was 7.5 mg SnO₂ per electrode in all cases, which is
28 controlled by continuous weighing of the electrode during the airbrushing process. Figure 1
29 shows a scheme of the as-prepared SnO₂-GDEs configuration.



1
2 **Fig. 1.** Graphical representation of the SnO₂-GDE configuration.
3

4 **2.3. Physicochemical and electrochemical characterization techniques.**

5 The crystalline structure of the SnO₂ NPs was analyzed by powder X-ray diffraction (XRD) on a
6 Bruker D8 Advance X-ray diffractometer in the 20-80° 2θ range using a Cu Kα X-ray irradiation
7 source (λ = 0.1542 nm). Step time and step size were 1 s and 0.03°, respectively. The specific
8 surface area analysis of the SnO₂ NPs was carried out by N₂ sorption at 77 K using a Belsorb
9 Max (Belsorb Japan). Prior to measurements, SnO₂ NPs were degassed for 15 h under a
10 primary vacuum at 150 °C. The BET method was applied to determine the specific surface area
11 of the electrocatalyst.

12 The morphology and the average size of the SnO₂ NPs were analyzed by high resolution
13 transmission electron microscopy (HR-TEM) using a JEOL 2100, which operates at 200 kV. The
14 samples were prepared by evaporating diluted suspensions in ethanol onto carbon-coated
15 copper grids. It is important to point out that more than 100 particles have been considered on
16 several TEM pictures in order to evaluate the average size of the as-prepared SnO₂ NPs.
17 Furthermore, the conductivity of the SnO₂ NPs was evaluated using impedance spectroscopy.
18 In brief, the conductivity was measured on ~14% SnO₂ NPs pellet (thickness = 1.21 mm and
19 diameter = 13 mm) at room temperature in air, with a frequency range varying between 0.1 and
20 10⁵ Hz and an amplitude of 200 mV_{rms} (4 repetitions). The spectra were then analyzed using
21 Zview software for the determination of the electrical conductivity of the SnO₂ NPs (Impedance
22 diagram shown in Figure S2).

23 Cyclic voltammetry (CV) analyses were performed using a CH Instruments 760E potentiostat in
24 a three-electrode configuration electrochemical cell. A glassy carbon (GC) electrode (3 mm in
25 diameter) was used as an inert current collector, at which different amounts of the prepared
26 suspension (SnO₂ NPs in isopropanol) were deposited by drop casting, whereas a graphite rod

1 and an Ag/AgCl (saturated in KCl) were used as the counter and the reference electrodes,
2 respectively. Either CO₂- or Ar-saturated 0.1 M KHCO₃ aqueous solutions were used as the
3 electrolyte. The pH of the above-mentioned electrolytes was experimentally measured being
4 6.98 ± 0.07 (CO₂ saturation) and 9.03 ± 0.10 (Ar saturation), respectively. The GC electrode
5 was mechanically polished with alumina, sonicated and rinsed with ultrapure water to ensure
6 the complete removal of SnO₂ NPs from previous experiments. The applied potential ranged
7 from 1 V to -1.75 V vs. Ag/AgCl at a scan rate of 100 mV s⁻¹. Potentials reported here were
8 converted to reversible hydrogen electrode (RHE) using the equation: $E_{\text{RHE}} = E_{\text{Ag/AgCl}} + 0.197 +$
9 0.059pH .

10

11 *2.4. CO₂ flow electrolyzer setup and experimental conditions*

12 The manufactured SnO₂-GDEs were tested for CO₂RR in an electrochemical filter-press reactor
13 configuration (Micro Flow Cell, Electrocell A/S) (see Figure S3), which operated at constant
14 current in continuous mode controlled by a MSTAT4 system (Arbin Instruments). The
15 electrochemical filter-press reactor was divided in two compartments (cathode and anode) by a
16 cationic exchange membrane Nafion® 117. The filter-press configuration can be found
17 elsewhere [63]. Figure 2 shows the CO₂RR continuous reactor scheme using a CO₂ single-pass
18 flow configuration. (0.5 M KCl + 0.45 M KHCO₃) and 1 M KOH aqueous solutions were used as
19 catholyte and anolyte, respectively. The effect on CO₂RR selectivity and performance of two
20 experimental parameters was evaluated: the electrolyte flow per geometric electrode area (F/A)
21 ($0.57, 0.15$ and $0.07 \text{ mL min}^{-1} \text{ cm}^{-2}$) and the applied current density (from 200 to 500 mA cm⁻²).
22 It is worth noting here that both the catholyte and the anolyte passed only once throughout the
23 cell (single-pass configuration). The cathode side was also fed with a pure CO₂ gas stream at a
24 flow of 200 mL min^{-1} . A Dimensionally Stable Anode [DSA/O₂ (Ir-MMO (mixed metal oxide) on
25 Pt)] and a leak-free Ag/AgCl 3.4 mol L⁻¹ KCl electrodes were used as the anode and the
26 reference, respectively. Reactor temperature was monitored along the experiment.

27 Liquid samples were analyzed by ion chromatography aiming at determining the formate
28 concentration. A Dionex ICS 1100 equipped with an AS9-HC column was used as ion
29 chromatograph, with a 4.5 mM Na₂CO₃ aqueous solution as the eluent (at a flow rate of 1 mL
30 min^{-1}) and operated at approximately 13.8 MPa. Some liquid samples were selected to analyze
31 the formation of alcohols by using a headspace gas chromatograph (GCMS-QP2010 Ultra
32 Shimadzu) equipped with a flame ionization detector (FID). Additionally, a four-channel gas
33 microchromatograph (490 Micro GC, Agilent Technologies) equipped with micro thermal
34 conductivity detectors (Micro-TCD) was used for the detection and quantification of gaseous
35 reduction products.

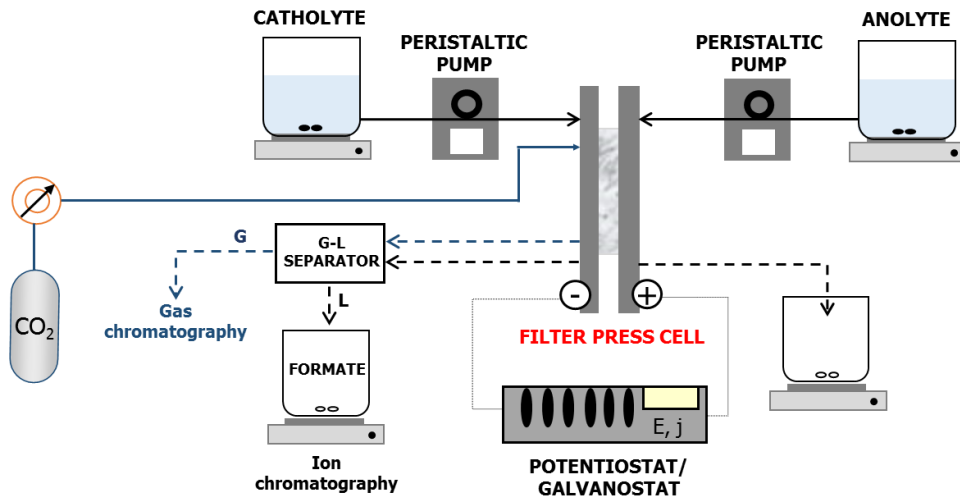


Fig. 2. CO₂RR continuous reactor setup scheme.

The manufactured SnO₂-GDEs were tested for continuous CO₂RR in a single-pass flow reactor at ambient conditions during 90 min electrolyses, where a pseudo-stable performance in time was observed (see Figure S4), as was previously described for Sn-GDEs [63]. Both liquid and gas samples were analyzed by duplicate every 30 min of electrolysis and an averaged concentration of each product (independent of electrolysis time) was calculated and reported herein. Some long-run electrolyses (5 h) were also performed to evaluate the stability of the developed electrocatalyst. Additionally, some figures of merit [66] to describe the CO₂RR were calculated, namely:

The Faradaic Efficiency (FE), which represents the percentage of the total charge applied to the system that is actually used to produce any target reduction product (*i.e.* formate), according to the following equation:

$$FE (\%) = \frac{z n F}{Q} \times 100 \quad (1)$$

where z represents the number of electrons exchanged to form the desired product (e.g. $z = 2$ for the electroconversion of CO₂ into formate), n corresponds to the number of moles produced, F is the Faraday constant ($F = 96,485 \text{ C mol}^{-1}$) and Q represents the total charge (C) circulated through the system, which is obtained by multiplying the current applied in amperes and the electrolysis time in seconds.

The Production Rate (r), which is defined as the productivity (moles) per unit of cathode area (geometric or electroactive area) and time ($\text{mmol m}^{-2} \text{ s}^{-1}$). r is essential to evaluate the technical feasibility of the process;

$$\text{Geometric rate} = r_G = F/A_G \cdot C_{\text{formate}} \quad (2)$$

$$\text{Real rate} = r_R = F/A_R \cdot C_{\text{formate}} \quad (3)$$

1 where (F/A) corresponds to the electrolyte flow per geometric (A_G) or real electrode area (A_R) in
2 $L\ m^{-2}\ s^{-1}$ and C_{formate} is the concentration of product detected in $mmol\ L^{-1}$.

3 The Energy Consumption (EC), which represents the required amount of energy used to
4 produce the target product (formate), according to:

$$5 \text{ Energy Consumption } \left(\frac{kWh}{kmol} \right) = \frac{Q \cdot V}{n} \times 2.78 \cdot 10^{-4} \quad (4)$$

6 where V represents the absolute cell potential in volts.

7 The Energy Efficiency (reported in Table S3), which represents the total energy used towards
8 the production of a specific desired product (e.g., formate), according to the following equation:

$$9 \text{ Energy Efficiency (\%)} = (E_T/E) \cdot FE \quad (5)$$

10 where E_T is the theoretical potential in volts required for the electrocatalytic reduction of CO_2 to
11 the product of interest (formate), whereas E and FE represent the real cathode potential applied
12 in volts and the formate Faradaic Efficiency (%), respectively.

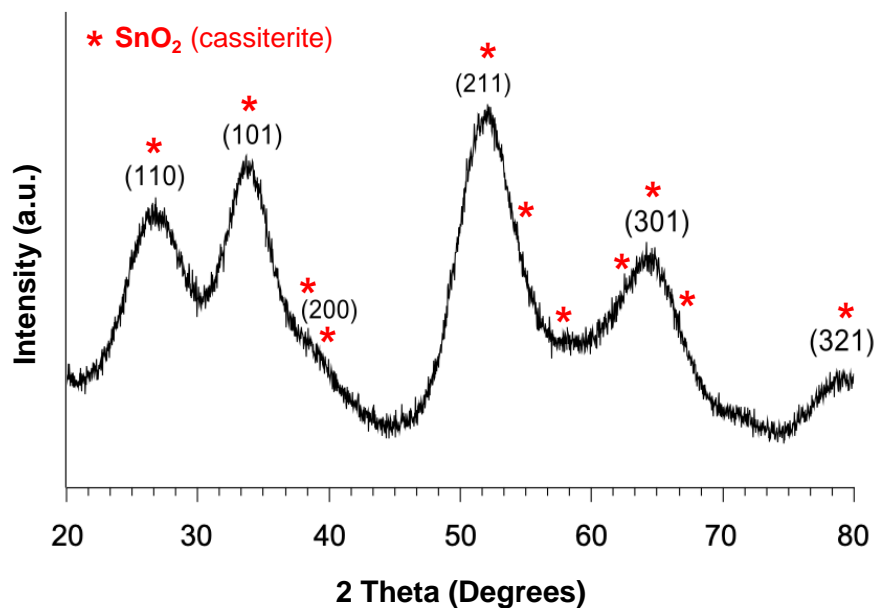
13

14 **3. Results and Discussion**

15 *3.1. Physicochemical characterization of SnO_2 nanoparticles*

16 The crystalline structure of the synthesized SnO_2 powder is firstly characterized using the X-ray
17 diffraction technique. The obtained pattern presented in Figure 3 is indexed with the tetragonal
18 phase of SnO_2 cassiterite (JCPDS 00-041-1445). The particle crystallite size is determined
19 using Scherrer method on several very broad diffraction lines (see Table S1) obtaining a very
20 small crystallite size, below 3 nm.

21

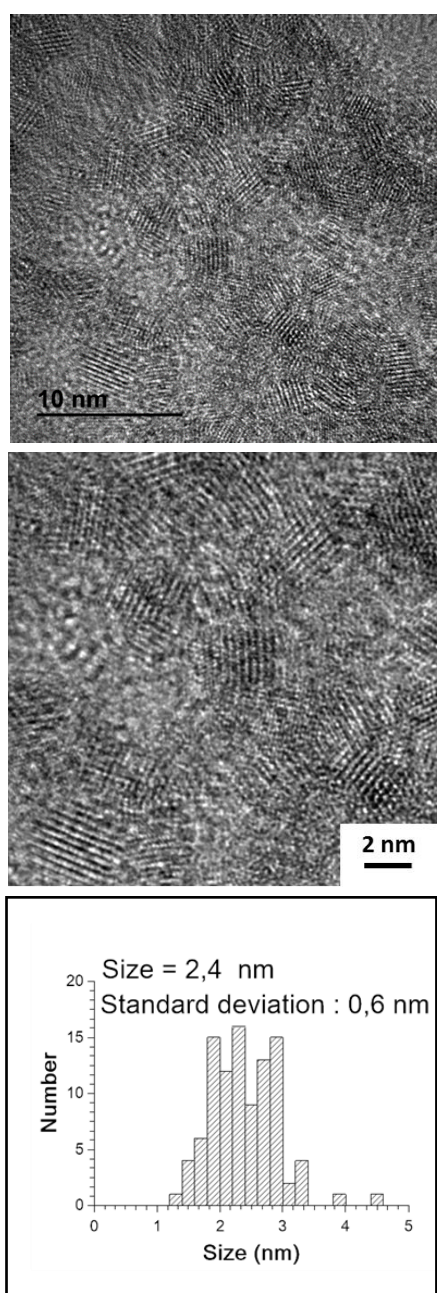


22

1
2
3
4
5
6
7
8
9
10

Fig. 3. X-ray diffraction pattern of the synthesized SnO₂ nanoparticles (the diffraction lines are indexed according to the cassiterite structure marked by red stars, JCPDS 00-041-1445).

This fact is further confirmed on the transmission electron micrographs of the synthesized SnO₂ NPs (Figure 4), where a mean size of (2.4 ± 0.6) nm can be measured. SnO₂ NPs are almost spherical and rather monodisperse in size. The surface area of the dried powder was also determined using the BET model and a specific surface area of (299 ± 10) m² g⁻¹ was determined for the synthesized SnO₂ NPs (see Figure S1), which is significantly larger than the value of commercially available equivalent nanomaterials.



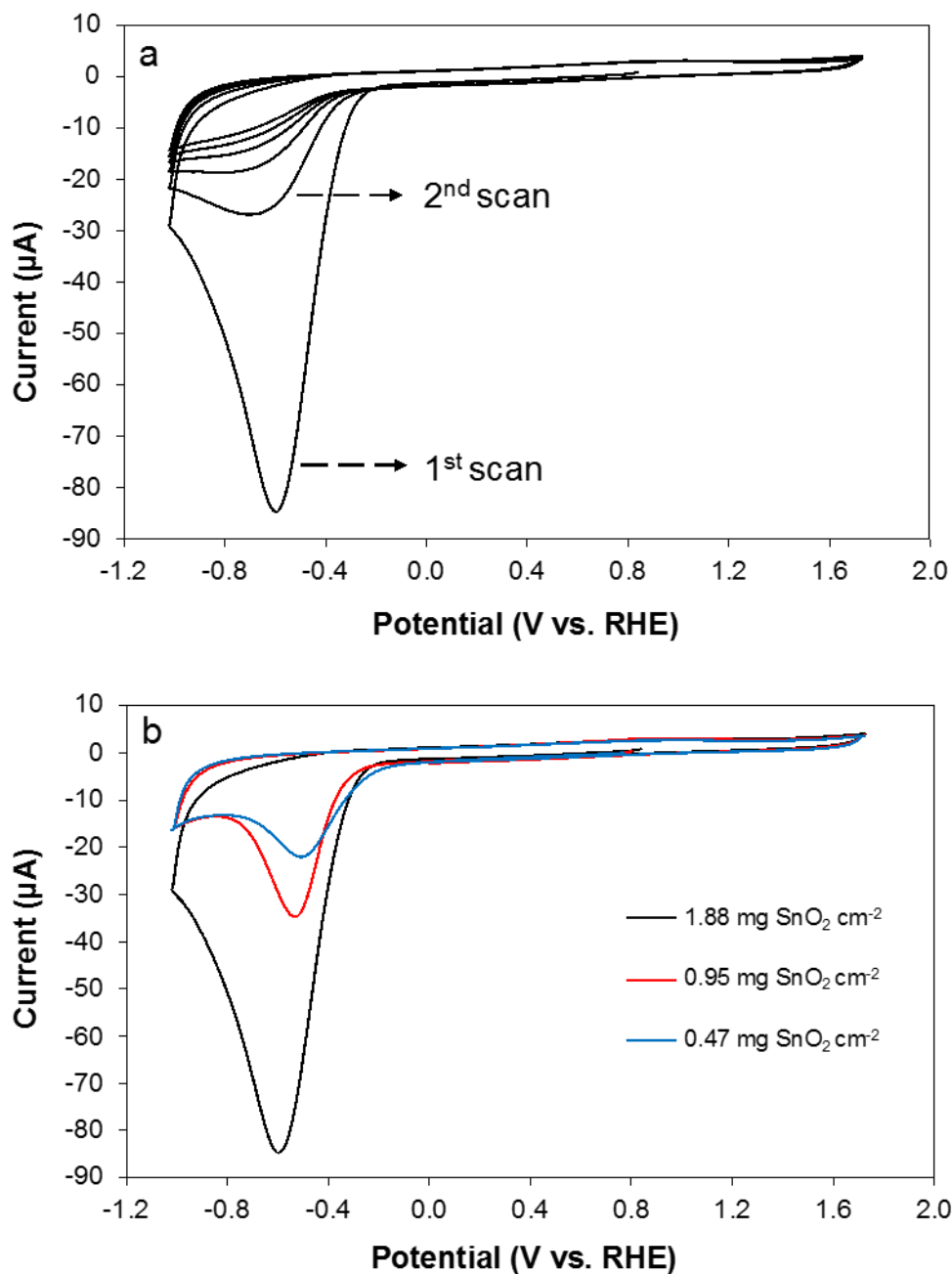
11
12

Fig. 4. HR-TEM image of synthesized SnO₂ nanoparticles including its size distribution.

1

2 3.2. Electrochemical characterization of SnO₂ nanoparticles

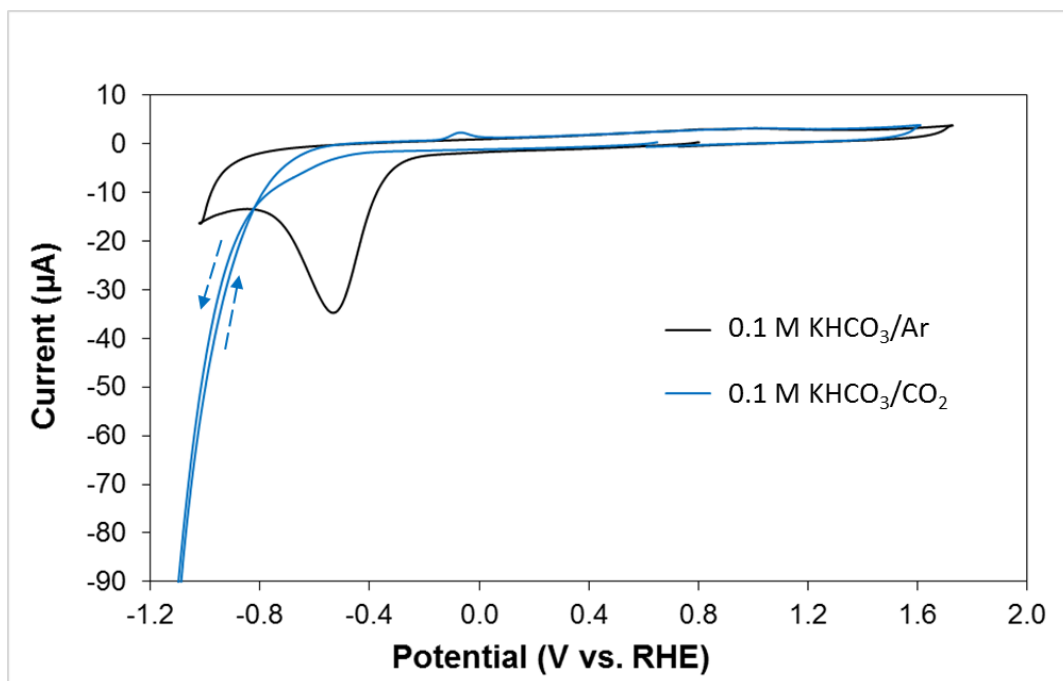
3 Different voltammetric analyses were carried out to study the electrochemical behavior of SnO₂
4 NPs in presence and absence of CO₂. In fact, some controversy is present in the literature
5 nowadays regarding the mechanism of CO₂RR on SnO₂, since some reports pointed out SnO₂
6 and SnO as catalytically active sites for CO₂RR [39,42,45], but others suggested an initial
7 electrochemical reduction step to form metallic Sn⁰, which was considered the actual catalytic
8 site [67]. We studied small aliquots of SnO₂/isopropanol suspension deposited onto a GC
9 electrode in presence and absence of CO₂. Figure 5a shows a clear and highly symmetrical
10 reduction peak centered at -0.53 V vs RHE in a CO₂ free solution, which decreases rapidly in
11 intensity with consecutive scans. This symmetrical peak shape denotes that the reduction
12 process has taken place on the electrode surface and it is not linked to any electroactive
13 species coming from the solution, which fits the reduction process from SnO₂ to metallic Sn⁰
14 previously reported by Zhang et al. [46]. Moreover, the backward scans show no reversibility in
15 the reduction process observed, since a negligible oxidation current is collected in the anodic
16 sweep. In addition to this, the effect of the amount of SnO₂ NPs deposited onto the electrode
17 surface was also studied in the first CV scan, as shown in Figure 5b. The electrochemical
18 response from the deposition of three different amounts of SnO₂ NPs (i.e. 1.88, 0.95 and 0.47
19 mg cm⁻²) was evaluated and lower peak currents were displayed as the amount of SnO₂
20 deposited decreases (8.5 10⁻⁵ A, 3.49 10⁻⁵ A and 2.20 10⁻⁵ A, respectively), which proves that
21 the reduction current observed is proportional to the amount of SnO₂ NPs on the electrode. In
22 contrast, Figure 6 shows a different electrochemical behavior displayed by SnO₂ NPs when CO₂
23 is present in solution. The reduction peak observed in figures 5a and 5b is not clearly shown,
24 which suggests a different reduction mechanism. A clear hysteresis is observed in the cyclic
25 voltammogram in the presence of CO₂ (blue plot in Figure 6), which denotes an electrode
26 surface modification when cathodic potential is applied, which is subsequently confirmed by the
27 presence of a symmetrical oxidation peak centered at -0.065 V in the anodic scan. This
28 oxidation peak could be attributed to the reoxidation of some metallic Sn⁰ previously formed
29 during the cathodic scan in agreement with Lee et al. [39] who have already demonstrated by
30 XRD and XPS the stability of large sized SnO₂ NPs during CO₂RR with only a small fraction of
31 metallic Sn⁰ formed at pH 8.4.



1

2 **Fig. 5.** Cyclic voltammetry of SnO_2 NPs deposited onto a GC electrode in an Ar saturated 0.1 M
 3 KHCO_3 aqueous solution: a) $1.88 \text{ mg SnO}_2 \text{ NPs cm}^{-2}$ are deposited and several consecutive
 4 scans are plotted, and b) effect of SnO_2 loading on the first CV scan to determine the peak
 5 currents. Scan rate 100 mV s^{-1} .

6

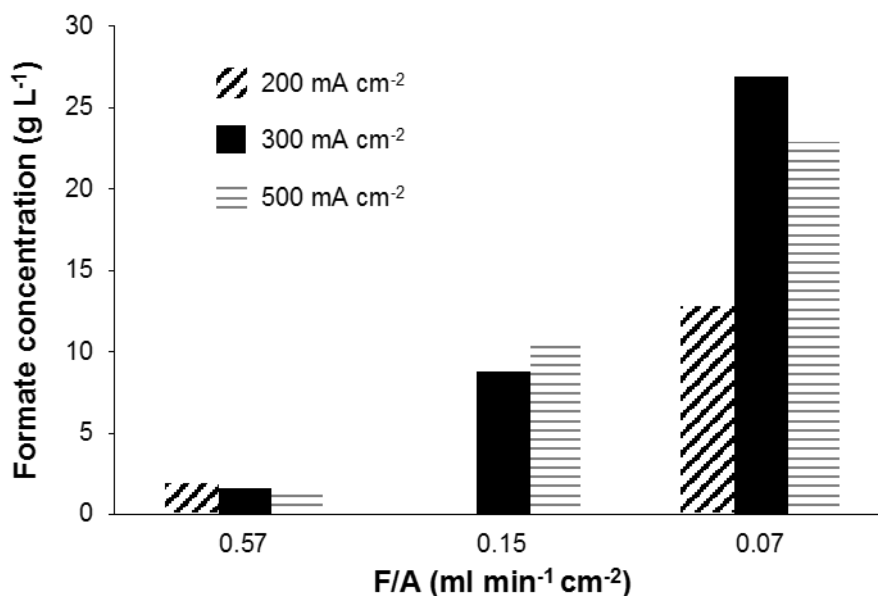


1
2 **Fig. 6.** Cyclic voltammetry of 0.95 mg SnO₂ NPs cm⁻² deposited onto a GC electrode in: (Black
3 plot) an Ar saturated 0.1 M KHCO₃ aqueous solution and (Blue plot) a CO₂ saturated 0.1 M
4 KHCO₃ aqueous solution. Scan rate 100 mV s⁻¹.

5
6 **3.3. Continuous CO₂ electroreduction into formate**

7 Two parameters were mainly evaluated on the performance of manufactured SnO₂-GDEs for
8 CO₂RR in a flow electrolyzer: the catholyte flow per geometric electrode area (F/A) (0.57, 0.15
9 and 0.07 mL min⁻¹ cm⁻²) and the applied current density (from 200 to 500 mA cm⁻²), since those
10 two operational variables were previously identified as key parameters in the production of
11 formate from CO₂RR [22,63,68]. Figure 7 shows that the production of formate, which is a key
12 figure of merit to evaluate the CO₂RR performance, is strongly dependent on both parameters:
13 F/A and current density. Figure 7 exhibits much higher formate concentrations for lower
14 catholyte flows per electrode area in all 3 current densities studied. This trend is in agreement
15 with previously reported results obtained using Sn-GDEs (10-15 nm Sn NPs) for CO₂RR in a
16 very similar flow electrolyzer at current densities between 90 and 200 mA cm⁻² [63].
17 Nevertheless, the comparison of formate concentration produced by equivalent experiments
18 performed at 200 mA cm⁻² in SnO₂-GDEs (1.8 and 12.9 g HCOO⁻ L⁻¹ at 0.57 and 0.07 mL min⁻¹
19 cm⁻², respectively) and Sn-GDEs (2.6 and 16.9 g HCOO⁻ L⁻¹ at 0.57 and 0.07 mL min⁻¹ cm⁻²,
20 respectively [63]) highlights a poorer formate productivity in SnO₂-GDEs, in spite of the fact that
21 SnO₂ NPs are significantly smaller in size than Sn NPs used in catalyzing the GDEs and SnO_x
22 have been identified as responsible of enhancing formate production. Thus, the electrical
23 conductivity of the synthesized SnO₂ NPs was evaluated by impedance spectroscopy (2 · 10⁻⁷ S
24 cm⁻¹). This conductivity value is typical in semiconducting materials such as SnO₂, but provokes
25 a significant electrical resistance in the electrode, which become more relevant at high current

1 densities. This fact was experimentally observed by heat generation in the reactor, which
 2 proved energy dissipation. This effect of the ohmic drop on electrode performance has been
 3 already addressed in flow electrolyzers for fuel cells [69]. Thus, an estimation of the impact in
 4 formate production by the electrical losses converted in heat by Joule effect during CO₂RR (*i.e.*,
 5 part of the charge supplied is used in generating heat instead of the reduction of CO₂ to the
 6 product of interest) was carried out and suggested that the difference in performance observed
 7 between SnO₂-GDEs and Sn-GDEs could be attributed to the moderate conductivity of SnO₂
 8 NPs. Some additional calculations are described in the supplementary information.



9

10 **Fig. 7.** Formate concentration produced on SnO₂-GDEs at different applied current densities
 11 and catholyte flows.

12 Table 1 presents the quantification of the main products in both liquid and gas-phases and the
 13 corresponding figures of merit obtained for CO₂RR performed on the manufactured SnO₂-GDEs
 14 in a flow electrolyzer at constant current. The most relevant result displayed in Table 1
 15 corresponds to a formate production of 27 g L⁻¹ (entry 5). This is the highest formate
 16 concentration value reported on Sn based electrocatalysts using a flow electrolyzer and a
 17 catholyte solution in equivalent conditions. Only catholyte-free electrolyzers have been able to
 18 produce significantly higher formate concentrations [68,70]. Table 2 compares the best results
 19 obtained in the present study and those previously reported in the literature achieved for SnO_x-
 20 GDE, Sn-GDE and Sn-catalyst coated membrane electrode (CCME) configurations in flow
 21 electrolyzers.

22

23

24

25

1 **Table 1.** Formate production rates, concentration, Faradaic efficiencies and energy
 2 consumption results at SnO₂-GDEs (metal loading = 0.75 mg cm⁻²) as a function of the current
 3 density and the catholyte flow.

Entry	Geometric current density, j_G (mA cm ⁻²)	F/A (mL min ⁻¹ cm ⁻²)	Geometric rate, r_G (mmol m ⁻² s ⁻¹)	Real rate, r_R (mmol m ⁻² s ⁻¹)	Formate concentration (g L ⁻¹)	Formate FE (%)	Energy consumption (kWh kmol ⁻¹)	Gas-phase FE (%)			
								H ₂	CO	C ₂ H ₄	C ₃ H ₈
1	200	0.57	3.9 ± 0.2	1.73 10 ⁻³ ± 6 10 ⁻⁵	1.8 ± 0.1	37.3 ± 1.4	933 ± 36	9.9 ± 1.0	0.33 ± 0.01	---	1.9 ± 0.4
2		0.07	3.3 ± 0.4	1.48 10 ⁻³ ± 2 10 ⁻⁴	12.9 ± 1.5	32.1 ± 3.7	1251 ± 141	30.0 ± 4.3	0.33 ± 0.01	---	0.5 ± 0.3
3	300	0.57	3.5 ± 0.2	1.57 10 ⁻³ ± 7 10 ⁻⁵	1.7 ± 0.1	22.6 ± 1.0	2013 ± 93	11.4 ± 1.5	0.25 ± 0.07	---	1.5 ± 0.2
4		0.15	4.9 ± 0.5	2.20 10 ⁻³ ± 2 10 ⁻⁴	8.8 ± 0.9	31.7 ± 3.2	1350 ± 142	7.7 ± 0.9	0.27 ± 0.06	---	0.3 ± 0.1
5		0.07	7.0 ± 0.1	3.11 10 ⁻³ ± 2 10 ⁻⁵	27.0 ± 0.2	44.9 ± 0.3	752 ± 4	8.7 ± 1.5	0.22 ± 0.01	---	1.0 ± 0.3
6	500	0.57	3.0 ± 0.8	1.34 10 ⁻³ ± 3 10 ⁻⁴	1.4 ± 0.4	11.6 ± 3.0	4392 ± 610	16.1 ± 1.1	0.10 ± 0.02	0.79 ± 0.1	0.95 ± 0.2
7		0.15	6.0 ± 0.1	2.68 10 ⁻³ ± 6 10 ⁻⁵	10.8 ± 0.3	23.2 ± 0.5	2194 ± 50	16.5 ± 1.1	0.10 ± 0.04	0.69 ± 0.1	0.67 ± 0.1
8		0.07	6.0 ± 0.2	2.65 10 ⁻³ ± 1 10 ⁻⁴	22.9 ± 0.9	23.0 ± 0.9	2266 ± 93	12.8 ± 1.0	0.10 ± 0.01	0.57 ± 0.1	0.96 ± 0.2

4

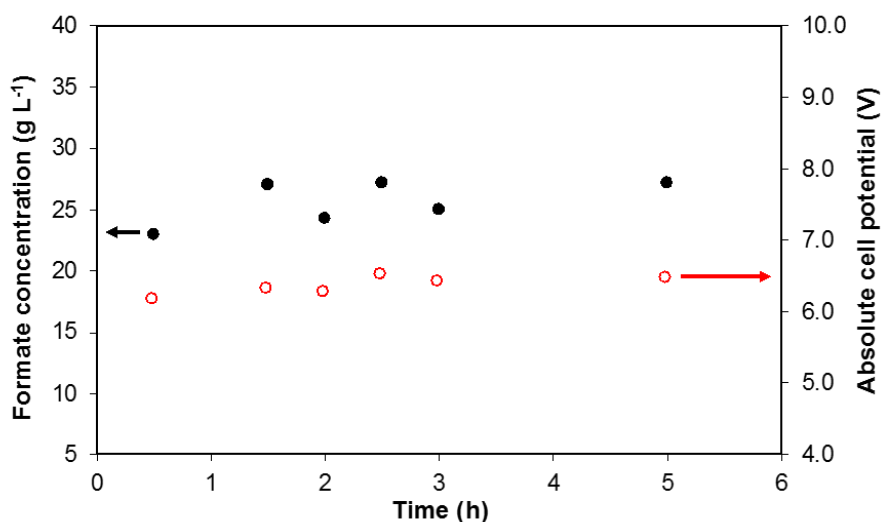
5 **Table 2.** Comparison of our highest CO₂-into-formate result on SnO₂-GDE and some examples
 6 from the literature on tin oxide-based GDE, Sn-GDE and Sn-CCME configurations, in all cases
 7 using flow electrolyzers.

Catalyst	Reactor configuration	Pressure (bar)	Temperature (K)	Geometric current density, j_G (mA cm ⁻²)	Formate concentration (g L ⁻¹)	Formate FE (%)
SnO ₂ -GDE (this work)	Divided single-pass	1	293	300	27	44.9
SnO ₂ -GDE [52]	Divided single-pass	1	293	385	1	72
SnO _x -GDE [53]	Divided single-pass	1	293	150	8.1	77
SnO-GDE [54]	Divided single-pass	1	293	300	10.5	81
Sn ₃ O ₄ -GDE [55]	Divided single-pass	1	293	462	-	91.1
Sn-GDE [63]	Divided single-pass	1	293	200	16.9	42.3
Sn-CCME [22]	Divided single-pass	1	293	45	19.2	49.4
Sn sheet [71]	Undivided Recirculation	30	293	80	19.2	
Sn-CCME [70]	Divided single-pass	1	343	55.4	41.5	93.3
Sn-CCME [70]	Divided single-pass	1	323	38.5	116.2	77.7

1 The catholyte flow per geometric electrode area (F/A) and the applied current density were the
2 two parameters evaluated on the results reported in Table 1. Looking first at the effect of current
3 density, two different behaviors can be observed. On the one hand, at high catholyte flow (5.7
4 mL min^{-1}) formate concentration remained unaffected by the applied current density, 1.8 , 1.7
5 and 1.4 g L^{-1} were detected at 200 , 300 and 500 mA cm^{-2} , respectively (entries 1, 3 and 6 in
6 Table 1). This fact provoked a relevant decrease in FE with increasing current density. On the
7 other hand, at low catholyte flow (0.7 mL min^{-1}) formate concentration, rate and FE described a
8 maximum at 300 mA cm^{-2} together with a minimum in EC of $752 \text{ kWh kmol}^{-1}$ (entry 5 in Table 1).
9 Additionally, the increase of applied current density at constant catholyte flow provoked a
10 significant diminution in the total FE of all quantified products, being 59.7% (entry 2) the
11 maximum value achieved among all results reported in Table 1. Looking at the effect of F/A
12 ratio in the results of Table 1, the formate concentration was significantly enhanced by reducing
13 F/A from 0.57 to $0.07 \text{ mL min}^{-1} \text{ cm}^{-2}$ in all 3 current densities. Nevertheless, two different
14 behaviors can be observed. On the one hand, at 200 mA cm^{-2} (entries 1 and 2 in Table 1)
15 formate concentration increased almost linearly (from 1.8 to 12.9 g L^{-1}) by decreasing F/A ratio
16 (from 0.57 to $0.07 \text{ mL min}^{-1} \text{ cm}^{-2}$) keeping FEs almost constant. On the other hand, at 300
17 (entries 3, 4 and 5 in Table 1) and 500 mA cm^{-2} (entries 6, 7 and 8 in Table 1) the increase
18 observed in formate concentration (from 1.7 to 27 g L^{-1} and from 1.4 to 22.9 g L^{-1} , respectively)
19 is twice the decrease in percentage of F/A ratio (from 0.57 to $0.07 \text{ mL min}^{-1} \text{ cm}^{-2}$). This fact
20 together with the diminution in the total FE of all quantified products when higher current
21 densities were applied and formate concentration independent of applied current density at high
22 catholyte flow clearly demonstrated the existence of a leakage of formate by crossover from the
23 catholyte towards the anolyte through the membrane, which was enhanced by increasing the
24 catholyte flow. This phenomenon of formate anions migration towards the anode is usually
25 negligible, working with a cationic exchange membrane like the one used in this work (Nafion
26 117), when the supporting electrolyte concentration (0.5 M) is significantly higher than the
27 formate generated in the catholyte and the cell potential between the electrodes does not
28 generate a strong electrical field. However, formate migration, which provokes the formate
29 crossover to the anolyte through the membrane and limits the maximum formate concentration
30 accumulated in the catholyte, becomes relevant when the concentration of formate generated
31 ($27 \text{ g L}^{-1} = 0.6 \text{ M}$) in the catholyte becomes higher than the supporting electrolyte concentration
32 (0.5 M), which happens when high current densities and low catholyte flow are applied. Then,
33 formate migration current contribution to the total current becomes highly significant. Actually, a
34 large drop in FE due to formate crossover through the Nafion 117 membrane was already
35 described when reducing CO_2 on a metallic Sn^0 electrode in a single pass flow reactor at high
36 applied current [38]. This effect together with the electrical resistance in the electrolyzer provoke
37 a poor total FE in all entries shown in Table 1, being poorer at higher current densities.

38 The stability and durability of the SnO_2 NPs catalyzing the CO_2RR on SnO_2 -GDEs represent an
39 important issue that needs to be addressed for evaluating the technical and economic feasibility
40 of the CO_2 electroconversion process. Therefore, Figure 8 shows the evolution of absolute cell

1 potential and formate concentration with electrolysis time under optimal conditions selected
 2 from Table 1 (300 mA cm^{-2} and $0.07 \text{ mL min}^{-1} \text{ cm}^{-2}$). Figure 8 exhibits an almost constant cell
 3 potential and production of formate with time, which demonstrates the long-term stability of
 4 SnO_2 NPs during CO_2 electroreduction. In particular, this cathode operated up to 10 h, in two
 5 independent, but consecutive electrolysis of 5 h each. The maximum standard deviation
 6 comparing the formate concentration quantified in the duplicate 5 h electrolysis is $\pm 0.4 \text{ g L}^{-1}$
 7 (see Table S2). Thus, the stability of the novel electrocatalyst proposed has been tested up to
 8 10 h including a STOP and START point in the middle. It is therefore worth recalling the
 9 significant formate concentration achieved after 5 h of electrolysis ($27 \text{ g L}^{-1} = 0.6 \text{ M}$) in
 10 comparison with metallic Sn^0 based catalysts from the literature (see Table 2), denoting the
 11 possibility of using size-controlled SnO_2 NPs with high specific surface area for an enhanced
 12 CO_2 electroconversion into formate. Moreover, this formate concentration is higher than the
 13 required one for the use of formate as a fuel in DFAFC for the generation of electricity, which
 14 has been reported to be, at least, 0.5 M [72]. Therefore, the use of high surface area SnO_2 NPs
 15 in flow electrolyzers may open a novel promising perspective to develop more robust systems
 16 for CO_2 electroconversion into formate combined with DFAFCs for energy production.



17

18 **Fig. 8.** Continuous formate production as a function of CO_2 electrolysis time on SnO_2 -GDE at
 19 300 mA cm^{-2} and $F/A = 0.07 \text{ mL min}^{-1} \text{ cm}^{-2}$, including absolute cell potential evolution with time.

20

Maximum formate concentration standard deviation: $\pm 0.4 \text{ g L}^{-1}$.

21

22 4. Conclusions

23 Crystalline and high specific surface area SnO_2 NPs (2.4 nm and $299 \text{ m}^2 \text{ g}^{-1}$ in average
 24 diameter size and surface area, respectively), synthesized by a facile hydrothermal microwave-
 25 assisted method, have been evaluated as an alternative electrocatalyst for the continuous
 26 production of formate from CO_2 single-pass electrochemical conversion, using large size
 27 electrodes operating at high current densities. So far, activity and selectivity performance of

1 SnO₂ NPs were reported either in a two compartments H-type cell displaying poor current
2 densities or in continuous flow electrolyzers using large size SnO₂ catalytic particles and small
3 size cathodes.

4 The electrochemical characterization by cyclic voltammetry of SnO₂ NPs has demonstrated a
5 different mechanism under CO₂ and Ar reduction conditions, since the reduction peak
6 associated with SnO₂ reduction to metallic Sn⁰ present in argon saturated solution is not clearly
7 shown in the presence of CO₂.

8 The effect of catholyte flow per geometric electrode area (F/A) (0.57, 0.15 and 0.07 mL min⁻¹
9 cm⁻²) and applied current density (200, 300 and 500 mA cm⁻²) were evaluated on the
10 performance of manufactured SnO₂-GDEs for continuous CO₂RR in a single-pass flow reactor
11 at ambient conditions. At a constant current density of 300 mA cm⁻² and low catholyte flow per
12 electrode area (0.07 mL min⁻¹ cm⁻²), a maximum formate concentration of 27 g L⁻¹ was achieved
13 with a FE of 44.9%, a formate production rate of 6.98 mmol m⁻² s⁻¹ and an energy consumption
14 of 752 kWh kmol⁻¹. This is the highest formate concentration value reported so far on Sn based
15 electrocatalysts using a flow electrolyzer and a catholyte solution in equivalent conditions. This
16 formate concentration result was only overcome by catholyte free flow electrolyzers, which
17 benefits from a minimal amount of water vapor present as catholyte to carry out the CO₂RR.
18 The FE towards formate using SnO₂ NPs was in the same range as those values reported for
19 Sn-based electrodes (40-50%), even though higher energy consumption per kmol of formate
20 produced was required at SnO₂-GDEs, which highlights the limited conductivity of SnO₂ NPs.

21 Poorer formate productivity in SnO₂-GDEs than in Sn-GDEs was observed at 200 mA cm⁻², in
22 spite of the fact that SnO₂ NPs were significantly smaller in size than Sn NPs and SnO_x have
23 been identified as responsible of enhancing formate production. This fact pointed out a non-
24 negligible ohmic drop contribution on the SnO₂-GDEs due to the semiconducting properties of
25 SnO₂, which provoked heat generation in the reactor by energy dissipation. However, the
26 electrical losses by Joule effect associated with the ohmic drop during CO₂RR were not large
27 enough to justify the low total FEs obtained (60 - 29 %), even though both liquid and gas-phase
28 products were analyzed. This fact together with the too high increase observed in formate
29 concentration linked to the decrease in F/A ratio at high current densities, as well as formate
30 production independent of applied current density observed at high catholyte flow,
31 demonstrated the existence of a leakage of formate by crossover migration from the catholyte
32 towards the anolyte through the membrane, which was enhanced by increasing the catholyte
33 flow. Formate migration limits the maximum formate concentration accumulated in the catholyte
34 in this work and becomes relevant because the concentration of formate generated (27 g L⁻¹ =
35 0.6 M) in the catholyte becomes higher than the supporting electrolyte concentration (0.5 M).
36 Then, formate migration current contribution to the total current becomes highly significant. For
37 this reason, using a higher supporting electrolyte concentration in the catholyte is envisaged for
38 the forthcoming experiments.

1 In conclusion, this study represents a step forward in the development of strategies based on
2 SnO₂ nanomaterials for the continuous electrochemical conversion of CO₂ into formate since a
3 formate concentration of 27 g L⁻¹ (0.6 M), which is superior to the limit for the use of formate as
4 a fuel in DFAFCs, has been achieved during 10 h (by 2 consecutive electrolysis of 5 h each) in
5 continuous galvanostatic mode at 300 mA cm⁻². Finally, these results suggest that interesting
6 future research may involve developing SnO₂-based electrodes displaying higher electrical
7 conductivity in order to reduce electrical losses and employing higher supporting electrolyte
8 concentrations in the catholyte combined with new ionic membrane separators able to reduce
9 the formate crossover from the catholyte to the anolyte where formate can be oxidized back to
10 CO₂. This will allow to significantly increase the efficiency of formate production from CO₂RR on
11 SnO₂ NPs at high current densities.

12

13 **Acknowledgements**

14 The authors gratefully acknowledge the financial sources from the Spanish Ministry of Economy
15 and Competitiveness (MINECO), through the project CTQ2016-76231-C2-1-R (AEI/FEDER,
16 UE). Moreover, I.M.-G. and C.M. S.-S would like to thank the MINECO for the postdoctoral
17 period in Paris of the predoctoral research contract (BES-2014-070081) and J. A. for the Ramón
18 y Cajal programme (RYC-2015-17080), respectively. L.T. and O.D. acknowledge the support of
19 French governmental funds managed by the ANR within the Investissements d'Avenir
20 programme under reference ANR-11-IDEX-0004-02, and more specifically within the framework
21 of the Cluster of Excellence MATISSE led by Sorbonne Université. Dr. G. Gouget is strongly
22 acknowledge for HR-TEM images.

23 **References**

- 24 [1] National Oceanic & Atmospheric Administration (NOAA), Trends in Atmospheric Carbon
25 Dioxide, Mauna Loa Observatory (MLO, Hawaii), Earth Syst. Res. Lab. (2020)
26 <https://www.esrl.noaa.gov/gmd/ccgg/trends/monthly>.
- 27 [2] X. Lu, D.Y.C. Leung, H. Wang, M.K.H. Leung, J. Xuan, Electrochemical Reduction of
28 Carbon Dioxide to Formic Acid, *ChemElectroChem*. 1 (2014) 836–849.
29 <https://doi.org/10.1002/celec.201300206>.
- 30 [3] J.T. Song, H. Song, B. Kim, J. Oh, Towards higher rate electrochemical CO₂ conversion:
31 From liquid-phase to gas-phase systems, *Catalysts*. 9 (2019) 224.
32 <https://doi.org/10.3390/catal9030224>.
- 33 [4] T. Sakakura, J.C. Choi, H. Yasuda, Transformation of carbon dioxide, *Chem. Rev.* 107
34 (2007) 2365–2387. <https://doi.org/10.1021/cr068357u>.
- 35 [5] I. Merino-Garcia, E. Alvarez-Guerra, J. Albo, A. Irabien, Electrochemical membrane
36 reactors for the utilisation of carbon dioxide, *Chem. Eng. J.* 305 (2016) 104–120.

- 1 <https://doi.org/10.1016/j.cej.2016.05.032>.
- 2 [6] J. Albo, M. Alvarez-Guerra, A. Irabien, Electro-, photo- and-photoelectro-chemical
3 reduction of CO₂, in: *Heterog. Catal. Emerg. Tech. Des. Charact. Appl.*, Wiley-VCH,
4 2020.
- 5 [7] J.L. White, M.F. Baruch, J.E. Pander, Y. Hu, I.C. Fortmeyer, J.E. Park, T. Zhang, K.
6 Liao, J. Gu, Y. Yan, T.W. Shaw, E. Abelev, A.B. Bocarsly, Light-Driven Heterogeneous
7 Reduction of Carbon Dioxide: Photocatalysts and Photoelectrodes, *Chem. Rev.* 115
8 (2015) 12888–12935. <https://doi.org/10.1021/acs.chemrev.5b00370>.
- 9 [8] A. Taheri, L.A. Berben, Making C-H bonds with CO₂: production of formate by molecular
10 electrocatalysts, *Chem. Commun.* 52 (2016) 1768–1777.
11 <https://doi.org/10.1039/c5cc09041e>.
- 12 [9] C. Costentin, M. Robert, J.M. Savéant, Catalysis of the electrochemical reduction of
13 carbon dioxide, *Chem. Soc. Rev.* 42 (2013) 2423–2436.
14 <https://doi.org/10.1039/c2cs35360a>.
- 15 [10] E.E. Benson, C.P. Kubiak, A.J. Sathrum, J.M. Smieja, Electrocatalytic and
16 homogeneous approaches to conversion of CO₂ to liquid fuels, *Chem. Soc. Rev.* 38
17 (2009) 89–99. <https://doi.org/10.1039/b804323j>.
- 18 [11] E. Vichou, Y. Li, M. Gomez-Mingot, M. Fontecave, C.M. Sánchez-Sánchez, Imidazolium-
19 And Pyrrolidinium-Based Ionic Liquids as Cocatalysts for CO₂ Electroreduction in Model
20 Molecular Electrocatalysis, *J. Phys. Chem. C.* 124 (2020) 23764–23772.
21 <https://doi.org/10.1021/acs.jpcc.0c07556>.
- 22 [12] S. Nitopi, E. Bertheussen, S.B. Scott, X. Liu, A.K. Engstfeld, S. Horch, B. Seger, I.E.L.
23 Stephens, K. Chan, C. Hahn, J.K. Nørskov, T.F. Jaramillo, I. Chorkendorff, Progress and
24 Perspectives of Electrochemical CO₂ Reduction on Copper in Aqueous Electrolyte,
25 *Chem. Rev.* 119 (2019) 7610–7672. <https://doi.org/10.1021/acs.chemrev.8b00705>.
- 26 [13] C.M. Sánchez-Sánchez, J. Souza-Garcia, E. Herrero, A. Aldaz, Electrocatalytic
27 reduction of carbon dioxide on platinum single crystal electrodes modified with adsorbed
28 adatoms, *J. Electroanal. Chem.* 668 (2012) 51–59.
29 <https://doi.org/10.1016/j.jelechem.2011.11.002>.
- 30 [14] L. Zhang, I. Merino-Garcia, J. Albo, C.M. Sánchez-Sánchez, Electrochemical CO₂
31 reduction reaction on cost-effective oxide-derived copper and transition metal–nitrogen–
32 carbon catalysts, *Curr. Opin. Electrochem.* 23 (2020) 65–73.
33 <https://doi.org/10.1016/j.coelec.2020.04.005>.
- 34 [15] H.K. Ju, G. Kaur, A.P. Kulkarni, S. Giddey, Challenges and trends in developing
35 technology for electrochemically reducing CO₂ in solid polymer electrolyte membrane
36 reactors, *J. CO₂ Util.* 32 (2019) 178–186. <https://doi.org/10.1016/j.jcou.2019.04.003>.

- 1 [16] R. Kortlever, J. Shen, K.J.P. Schouten, F. Calle-Vallejo, M.T.M. Koper, Catalysts and
2 Reaction Pathways for the Electrochemical Reduction of Carbon Dioxide, *J. Phys.*
3 *Chem. Lett.* 6 (2015) 4073–4082. <https://doi.org/10.1021/acs.jpcllett.5b01559>.
- 4 [17] C.M. Sánchez-Sánchez, V. Montiel, D.A. Tryk, A. Aldaz, A. Fujishima, Electrochemical
5 approaches to alleviation of the problem of carbon dioxide accumulation, *Pure Appl.*
6 *Chem.* 73 (2001) 1917–1927. <https://doi.org/10.1351/pac200173121917>.
- 7 [18] J. Wu, Y. Huang, W. Ye, Y. Li, CO₂ Reduction: From the Electrochemical to
8 Photochemical Approach, *Adv. Sci.* 4 (2017) 1700194.
9 <https://doi.org/10.1002/advs.201700194>.
- 10 [19] J. Qiao, Y. Liu, F. Hong, J. Zhang, A review of catalysts for the electroreduction of
11 carbon dioxide to produce low-carbon fuels, *Chem. Soc. Rev.* 43 (2014) 631–675.
12 <https://doi.org/10.1039/c3cs60323g>.
- 13 [20] C. Delacourt, P.L. Ridgway, J.B. Kerr, J. Newman, Design of an Electrochemical Cell
14 Making Syngas (CO +H₂) from CO₂ and H₂O Reduction at Room Temperature, *J.*
15 *Electrochem. Soc.* 155 (2007) B42–B49. <https://doi.org/10.1149/1.2801871>.
- 16 [21] I. Merino-Garcia, J. Albo, P. Krzywda, G. Mul, A. Irabien, Bimetallic Cu-based hollow
17 fibre electrodes for CO₂ electroreduction, *Catal. Today.* 346 (2020) 34–39.
18 <https://doi.org/10.1016/j.cattod.2019.03.025>.
- 19 [22] G. Díaz-Sainz, M. Alvarez-Guerra, J. Solla-Gullón, L. García-Cruz, V. Montiel, A. Irabien,
20 Catalyst coated membrane electrodes for the gas phase CO₂ electroreduction to
21 formate, *Catal. Today.* 346 (2020) 58–64. <https://doi.org/10.1016/j.cattod.2018.11.073>.
- 22 [23] J. García, C. Jiménez, F. Martínez, R. Camarillo, J. Rincón, Electrochemical reduction of
23 CO₂ using Pb catalysts synthesized in supercritical medium, *J. Catal.* 367 (2018) 72–80.
24 <https://doi.org/10.1016/j.jcat.2018.08.017>.
- 25 [24] J. Albo, A. Sáez, J. Solla-Gullón, V. Montiel, A. Irabien, Production of methanol from
26 CO₂ electroreduction at Cu₂O and Cu₂O/ZnO-based electrodes in aqueous solution,
27 *Appl. Catal. B Environ.* 176–177 (2015) 709–717.
28 <https://doi.org/10.1016/j.apcatb.2015.04.055>.
- 29 [25] D. Ren, Y. Deng, A.D. Handoko, C.S. Chen, S. Malkhandi, B.S. Yeo, Selective
30 Electrochemical Reduction of Carbon Dioxide to Ethylene and Ethanol on Copper(I)
31 oxide catalysts, *ACS Catal.* 5 (2015) 2814–2821. <https://doi.org/10.1021/cs502128q>.
- 32 [26] I. Merino-Garcia, J. Albo, A. Irabien, Productivity and Selectivity of Gas-Phase CO₂
33 Electroreduction to Methane at Copper Nanoparticle-Based Electrodes, *Energy Technol.*
34 5 (2017) 922–928. <https://doi.org/10.1002/ente.201600616>.
- 35 [27] I. Merino-Garcia, J. Albo, J. Solla-Gullón, V. Montiel, A. Irabien, Cu oxide/ZnO-based

- 1 surfaces for a selective ethylene production from gas-phase CO₂ electroconversion, *J.*
2 *CO₂ Util.* 31 (2019) 135–142. <https://doi.org/10.1016/j.jcou.2019.03.002>.
- 3 [28] Z. Cai, Y. Wu, Z. Wu, L. Yin, Z. Weng, Y. Zhong, W. Xu, X. Sun, H. Wang, Unlocking
4 bifunctional electrocatalytic activity for CO₂ reduction reaction by win-win metal-oxide
5 cooperation, *ACS Energy Lett.* 3 (2018) 2816–2822.
6 <https://doi.org/10.1021/acsenergylett.8b01767>.
- 7 [29] X. Yu, P.G. Pickup, Recent advances in direct formic acid fuel cells (DFAFC), *J. Power*
8 *Sources.* 182 (2008) 124–132. <https://doi.org/10.1016/j.jpowsour.2008.03.075>.
- 9 [30] S. Ponnurangam, I. V. Chernyshova, P. Somasundaran, Nitrogen-containing polymers
10 as a platform for CO₂ electroreduction, *Adv. Colloid Interface Sci.* 244 (2017) 184–198.
11 <https://doi.org/10.1016/j.cis.2016.09.002>.
- 12 [31] C. Oloman, H. Li, Electrochemical processing of carbon dioxide, *ChemSusChem.* 1
13 (2008) 385–391. <https://doi.org/10.1002/cssc.200800015>.
- 14 [32] U.O. Nwabara, E.R. Cofell, S. Verma, E. Negro, P.J.A. Kenis, Durable Cathodes and
15 Electrolyzers for the Efficient Aqueous Electrochemical Reduction of CO₂,
16 *ChemSusChem.* 13 (2020) 855–875. <https://doi.org/10.1002/cssc.201902933>.
- 17 [33] A. Irabien, M. Alvarez-Guerra, J. Albo, A. Dominguez-Ramos, Electrochemical
18 conversion of CO₂ to value-added products, in: *Electrochem. Water Wastewater Treat.*,
19 Elsevier, Amsterdam, 2018: pp. 29–59.
- 20 [34] N. Han, P. Ding, L. He, Y. Li, Y. Li, Promises of Main Group Metal-Based
21 Nanostructured Materials for Electrochemical CO₂ Reduction to Formate, *Adv. Energy*
22 *Mater.* 10 (2020) 1902338. <https://doi.org/10.1002/aenm.202070046>.
- 23 [35] G. Díaz-Sainz, M. Alvarez-Guerra, J. Solla-Gullón, L. García-Cruz, V. Montiel, A. Irabien,
24 CO₂ electroreduction to formate: Continuous single-pass operation in a filter-press
25 reactor at high current densities using Bi gas diffusion electrodes, *J. CO₂ Util.* 34 (2019)
26 12–19. <https://doi.org/10.1016/j.jcou.2019.05.035>.
- 27 [36] D. Wu, G. Huo, W.Y. Chen, X.Z. Fu, J.L. Luo, Boosting formate production at high
28 current density from CO₂ electroreduction on defect-rich hierarchical mesoporous
29 Bi/Bi₂O₃ junction nanosheets, *Appl. Catal. B Environ.* 271 (2020) 118957.
30 <https://doi.org/10.1016/j.apcatb.2020.118957>.
- 31 [37] D. Pavesi, R.C.J. Van De Poll, J.L. Krasovic, M. Figueiredo, G.J.M. Gruter, M.T.M.
32 Koper, K.J.P. Schouten, Cathodic Disintegration as an Easily Scalable Method for the
33 Production of Sn-and Pb-Based Catalysts for CO₂Reduction, *ACS Sustain. Chem. Eng.*
34 8 (2020) 15603–15610. <https://doi.org/10.1021/acssuschemeng.0c04875>.
- 35 [38] H. Li, C. Oloman, Development of a continuous reactor for the electro-reduction of

- 1 carbon dioxide to formate - Part 2: Scale-up, *J. Appl. Electrochem.* 37 (2007) 1107–
2 1117. <https://doi.org/10.1007/s10800-007-9371-8>.
- 3 [39] S. Lee, J.D. Ocon, Y. Il Son, J. Lee, Alkaline CO₂ electrolysis toward selective and
4 continuous HCOO⁻ production over SnO₂ nanocatalysts, *J. Phys. Chem. C.* 119 (2015)
5 4884–4890. <https://doi.org/10.1021/jp512436w>.
- 6 [40] B. Kumar, V. Atla, J.P. Brian, S. Kumari, T.Q. Nguyen, M. Sunkara, J.M. Spurgeon,
7 Reduced SnO₂ Porous Nanowires with a High Density of Grain Boundaries as Catalysts
8 for Efficient Electrochemical CO₂-into-HCOOH Conversion, *Angew. Chemie - Int. Ed.* 56
9 (2017) 3645–3649. <https://doi.org/10.1002/anie.201612194>.
- 10 [41] Y. Chen, M.W. Kanan, Tin oxide dependence of the CO₂ reduction efficiency on tin
11 electrodes and enhanced activity for tin/tin oxide thin-film catalysts, *J. Am. Chem. Soc.*
12 134 (2012) 1986–1989. <https://doi.org/10.1021/ja2108799>.
- 13 [42] Yiliguma, Z. Wang, C. Yang, A. Guan, L. Shang, A.M. Al-Enizi, L. Zhang, G. Zheng, Sub-
14 5 nm SnO₂ chemically coupled hollow carbon spheres for efficient electrocatalytic CO₂
15 reduction, *J. Mater. Chem. A.* 6 (2018) 20121–20127.
16 <https://doi.org/10.1039/c8ta08058e>.
- 17 [43] C. Zhao, J. Wang, J.B. Goodenough, Comparison of electrocatalytic reduction of CO₂ to
18 HCOOH with different tin oxides on carbon nanotubes, *Electrochem. Commun.* 65
19 (2016) 9–13. <https://doi.org/10.1016/j.elecom.2016.01.019>.
- 20 [44] R. Zhang, W. Lv, L. Lei, Role of the oxide layer on Sn electrode in electrochemical
21 reduction of CO₂ to formate, *Appl. Surf. Sci.* 356 (2015) 24–29.
22 <https://doi.org/10.1016/j.apsusc.2015.08.006>.
- 23 [45] Y. Fu, Y. Li, X. Zhang, Y. Liu, J. Qiao, J. Zhang, D.P. Wilkinson, Novel hierarchical SnO₂
24 microsphere catalyst coated on gas diffusion electrode for enhancing energy efficiency
25 of CO₂ reduction to formate fuel, *Appl. Energy.* 175 (2016) 536–544.
26 <https://doi.org/10.1016/j.apenergy.2016.03.115>.
- 27 [46] S. Zhang, P. Kang, T.J. Meyer, Nanostructured tin catalysts for selective electrochemical
28 reduction of carbon dioxide to formate, *J. Am. Chem. Soc.* 136 (2014) 1734–1737.
29 <https://doi.org/10.1021/ja4113885>.
- 30 [47] J. Wu, F.G. Risalvato, S. Ma, X.D. Zhou, Electrochemical reduction of carbon dioxide III.
31 The role of oxide layer thickness on the performance of Sn electrode in a full
32 electrochemical cell, *J. Mater. Chem. A.* 2 (2014) 1647–1651.
33 <https://doi.org/10.1039/c3ta13544f>.
- 34 [48] A. Kuzume, A. Dutta, S. Vesztegom, P. Broekmann, Operando raman spectroscopy:
35 Studies on the Reactivity and Stability of SnO₂ Nanoparticles During Electrochemical
36 CO₂ Reduction Reaction, in: *Encycl. Interfacial Chem. Surf. Sci. Electrochem.*, Elsevier,

- 1 2018: pp. 217–226. <https://doi.org/10.1016/B978-0-12-409547-2.13300-1>.
- 2 [49] M.F. Baruch, J.E. Pander, J.L. White, A.B. Bocarsly, Mechanistic Insights into the
3 Reduction of CO₂ on Tin Electrodes using in Situ ATR-IR Spectroscopy, *ACS Catal.* 5
4 (2015) 3148–3156. <https://doi.org/10.1021/acscatal.5b00402>.
- 5 [50] A. Dutta, A. Kuzume, M. Rahaman, S. Vesztergom, P. Broekmann, Monitoring the
6 Chemical State of Catalysts for CO₂ Electroreduction: An In Operando Study, *ACS*
7 *Catal.* 5 (2015) 7498–7502. <https://doi.org/10.1021/acscatal.5b02322>.
- 8 [51] F.D. Mayer, P. Hosseini-Benhangi, C.M. Sánchez-Sánchez, E. Asselin, E.L. Gyenge,
9 Scanning electrochemical microscopy screening of CO₂ electroreduction activities and
10 product selectivities of catalyst arrays, *Commun. Chem.* 3 (2020) 155.
11 <https://doi.org/10.1038/s42004-020-00399-6>.
- 12 [52] S. Sen, S.M. Brown, M.L. Leonard, F.R. Brushett, Electroreduction of carbon dioxide to
13 formate at high current densities using tin and tin oxide gas diffusion electrodes, *J. Appl.*
14 *Electrochem.* 49 (2019) 917–928. <https://doi.org/10.1007/s10800-019-01332-z>.
- 15 [53] M. Li, M.N. Idros, Y. Wu, S. Garg, S. Gao, R. Lin, H. Rabiee, Z. Li, L. Ge, T.E. Rufford,
16 Z. Zhu, L. Li, G. Wang, Unveiling the effects of dimensionality of tin oxide-derived
17 catalysts on CO₂ reduction by using gas-diffusion electrodes, *React. Chem. Eng.* 6
18 (2021) 345–352. <https://doi.org/10.1039/d0re00396d>.
- 19 [54] Y. Qian, Y. Liu, H. Tang, B.L. Lin, Highly efficient electroreduction of CO₂ to formate by
20 nanorod@2D nanosheets SnO, *J. CO₂ Util.* 42 (2020) 101287.
21 <https://doi.org/10.1016/j.jcou.2020.101287>.
- 22 [55] L.X. Liu, Y. Zhou, Y.C. Chang, J.R. Zhang, L.P. Jiang, W. Zhu, Y. Lin, Tuning Sn₃O₄ for
23 CO₂ reduction to formate with ultra-high current density, *Nano Energy.* 77 (2020)
24 105296. <https://doi.org/10.1016/j.nanoen.2020.105296>.
- 25 [56] G. Liu, Z. Li, J. Shi, K. Sun, Y. Ji, Z. Wang, Y. Qiu, Y. Liu, Z. Wang, P.A. Hu, Black
26 reduced porous SnO₂ nanosheets for CO₂ electroreduction with high formate selectivity
27 and low overpotential, *Appl. Catal. B Environ.* 260 (2020) 118134.
28 <https://doi.org/10.1016/j.apcatb.2019.118134>.
- 29 [57] F. Li, L. Chen, G.P. Knowles, D.R. MacFarlane, J. Zhang, Hierarchical Mesoporous
30 SnO₂ Nanosheets on Carbon Cloth: A Robust and Flexible Electrocatalyst for CO₂
31 Reduction with High Efficiency and Selectivity, *Angew. Chemie.* 56 (2017) 505–509.
32 <https://doi.org/10.1002/ange.201608279>.
- 33 [58] E. Jeng, F. Jiao, Investigation of CO₂ single-pass conversion in a flow electrolyzer,
34 *React. Chem. Eng.* 5 (2020) 1768–1775. <https://doi.org/10.1039/d0re00261e>.
- 35 [59] S. Malkhandi, B.S. Yeo, Electrochemical conversion of carbon dioxide to high value

- 1 chemicals using gas-diffusion electrodes, *Curr. Opin. Chem. Eng.* 26 (2019) 112–121.
2 <https://doi.org/10.1016/j.coche.2019.09.008>.
- 3 [60] P. Jeanty, C. Scherer, E. Magori, K. Wiesner-Fleischer, O. Hinrichsen, M. Fleischer,
4 Upscaling and continuous operation of electrochemical CO₂ to CO conversion in
5 aqueous solutions on silver gas diffusion electrodes, *J. CO₂ Util.* 24 (2018) 454–462.
6 <https://doi.org/10.1016/j.jcou.2018.01.011>.
- 7 [61] B.L. Caetano, F. Meneau, C. V. Santilli, S.H. Pulcinelli, M. Magnani, V. Briois,
8 Mechanisms of SnO₂ nanoparticles formation and growth in acid ethanol solution
9 derived from SAXS and combined raman-XAS time-resolved studies, *Chem. Mater.* 26
10 (2014) 6777–6785. <https://doi.org/10.1021/cm5032688>.
- 11 [62] M. Krishna, S. Komarneni, Conventional- vs microwave-hydrothermal synthesis of tin
12 oxide, SnO₂ nanoparticles, *Ceram. Int.* 35 (2009) 3375–3379.
13 <https://doi.org/10.1016/j.ceramint.2009.06.010>.
- 14 [63] A. Del Castillo, M. Alvarez-Guerra, J. Solla-Gullón, A. Sáez, V. Montiel, A. Irabien, Sn
15 nanoparticles on gas diffusion electrodes: Synthesis, characterization and use for
16 continuous CO₂ electroreduction to formate, *J. CO₂ Util.* 18 (2017) 222–228.
17 <https://doi.org/10.1016/j.jcou.2017.01.021>.
- 18 [64] G. Díaz-Sainz, M. Alvarez-Guerra, B. Ávila-Bolívar, J. Solla-Gullón, V. Montiel, A.
19 Irabien, Improving trade-offs in the figures of merit of gas-phase single-pass continuous
20 CO₂ electrocatalytic reduction to formate, *Chem. Eng. J.* 405 (2021) 126965.
21 <https://doi.org/10.1016/j.cej.2020.126965>.
- 22 [65] A. Del Castillo, M. Alvarez-Guerra, J. Solla-Gullón, A. Sáez, V. Montiel, A. Irabien,
23 Electrocatalytic reduction of CO₂ to formate using particulate Sn electrodes: Effect of
24 metal loading and particle size, *Appl. Energy.* 157 (2015) 165–173.
25 <https://doi.org/10.1016/j.apenergy.2015.08.012>.
- 26 [66] C.M. Sánchez-Sánchez, E. Expósito, J. Solla-Gullón, V. García-García, V. Montiel, A.
27 Aldaz, Calculation of the characteristic performance indicators in an electrochemical
28 process, *J. Chem. Educ.* 80 (2003) 529. <https://doi.org/10.1021/ed080p529>.
- 29 [67] J. Gu, F. Héroguel, J. Luterbacher, X. Hu, Densely Packed, Ultra Small SnO
30 Nanoparticles for Enhanced Activity and Selectivity in Electrochemical CO₂ Reduction,
31 *Angew. Chemie - Int. Ed.* 57 (2018) 2943–2947. <https://doi.org/10.1002/anie.201713003>.
- 32 [68] G. Díaz-Sainz, M. Alvarez-Guerra, A. Irabien, Continuous electrochemical reduction of
33 CO₂ to formate: Comparative study of the influence of the electrode configuration with
34 Sn and Bi-based electrocatalysts, *Molecules.* 25 (2020) 4457.
35 <https://doi.org/10.3390/molecules25194457>.
- 36 [69] Y. Bultel, P. Ozil, R. Durand, Modelling the mode of operation of PEMFC electrodes at

- 1 the particle level: Influence of ohmic drop within the active layer on electrode
2 performance, *J. Appl. Electrochem.* 28 (1998) 269–276.
3 <https://doi.org/10.1023/A:1003207514936>.
- 4 [70] W. Lee, Y.E. Kim, M.H. Youn, S.K. Jeong, K.T. Park, Catholyte-Free Electrocatalytic
5 CO₂ Reduction to Formate, *Angew. Chemie - Int. Ed.* 57 (2018) 6883–6887.
6 <https://doi.org/10.1002/anie.201803501>.
- 7 [71] F. Proietto, B. Schiavo, A. Galia, O. Scialdone, Electrochemical conversion of CO₂ to
8 HCOOH at tin cathode in a pressurized undivided filter-press cell, *Electrochim. Acta.* 277
9 (2018) 30–40. <https://doi.org/10.1016/j.electacta.2018.04.159>.
- 10 [72] L. An, R. Chen, Direct formate fuel cells: A review, *J. Power Sources.* 320 (2016) 127–
11 139. <https://doi.org/10.1016/j.jpowsour.2016.04.082>.
- 12